Available online at www.sciencedirect.com
ScienceDirect
Journal of Sound and Vibration 316 (2008) 69–86
JOURNAL OF SOUND AND VIBRATION
www.elsevier.com/locate/jsvi

Dynamic response of a pseudoelastic shape memory alloy beam to a moving load

A.A. Jafari, H. Ghiasvand*

Department of Mechanical Engineering, K.N. Toosi University of Technology, P.O. Box 19395-1999, Tehran, Iran

Received 25 June 2007; received in revised form 13 February 2008; accepted 26 February 2008
Handling Editor: A.V. Metrikine
Available online 8 April 2008

Abstract

This paper presents the dynamic response of multi-span shape memory alloy (SMA) beams subjected to a moving load. The behavior of an SMA beam is analyzed for the case of pseudoelasticity on the basis of an extended one-dimensional constitutive model. Lagrange's equations are applied to analyze dynamic response of the beam. A trial function representing the deflection of the beam is expressed in the polynomial form. Hysteresis-induced damping effect, variations of Young's modulus and natural frequencies of the beam due to stress-induced phase transformation (SIPT) are studied. The results of numerical simulations are presented for single-span and two-span SMA beams in different types of motions and load speeds, load amplitudes and damping effects. The numerical investigations show that the developed model is an effective computational tool for the simulation of dynamic response of the pseudoelastic SMA beams subjected to moving loads.

1. Introduction

Several characteristics of Nitinol shape memory alloys (NiTi SMAs) make them useful for innovative applications. These characteristics are: (1) large elastic strain range; (2) hysteretic damping; (3) highly reliable energy dissipation based on a repeatable solid-state phase transformation; (4) strain hardening at strains above 6%; (5) excellent low- and high-cycle fatigue properties and (6) excellent corrosion resistance. The pseudoelastic SMA element can provide a restoring force to recover its original condition after deformation. The pseudoelastic behavior of NiTi SMAs is a unique hysteretic energy-dissipation behavior, which makes NiTi SMA a viable candidate for passive or structural vibration control applications [1]. Also, the loss of stiffness of SMAs during phase transformation makes them useful as absorbers or vibration dampers, for example, in seismic applications [2]. However, it is important to develop an in-depth understanding of NiTi's behavior under dynamic loads. The researches carried out in this area have been very limited. Some of the practical examples associated with this subject are as follows: Damping behavior, loss of stiffness, dissipation energy and deformation of the SMA raw material (rod) in the cutting zone during the machining process are

*Corresponding author. Tel.: +98 2177937278.
E-mail address: h_ghsvnd@yahoo.com (H. Ghiasvand).

0022-460X/$ - see front matter © 2008 Elsevier Ltd. All rights reserved.
doi:10.1016/j.jsv.2008.02.042

Nomenclature

c	maximum value of moving load velocity
c_{cr}	critical velocity
DDD	dimensionless dynamic deflection
E	equivalent Young's modulus of SMA
E_A	Young's modulus of the austenite phase
E_S	Young's modulus of the martensite phase
F_0	amplitude of the concentrated moving load
x_F	moving load position at any time
w_{st}	static deflection at the midpoint of a simply supported SMA beam with full austenite phase subjected to concentrated force F_0 at the same point
$w(x,t)$	displacement function of the beam
α	dimensionless speed parameter
ξ	dimensionless equivalent damping ratio
ξ_S	volumetric fraction of the martensite phase
η	loss factor
σ_s^{AS}	initiated stress of forward phase transformation ($A \rightarrow S$)
σ_f^{AS}	finished stress of forward phase transformation
σ_s^{SA}	initiated stress of the reverse phase transformation ($S \rightarrow A$)
σ_f^{SA}	finished stress of the reverse phase transformation
ω_k	natural circular frequency of the kth mode

important data for the stability analysis of the cutting process. Chatter is a difficult problem that affects the stability of the cutting process and may be decreased by the damping behavior of the SMA material. Undesired and large deformations of any structure such as railways or highways bridges subjected to moving loads can be reduced effectively by using SMA as a damping element of the structure. Using pseudoelastic SMA restrainer bars in a bridge structure has been noted by Des Roches and Delemant [3]. They concluded that the SMA restrainers reduce relative hinge displacements at the abutment much more effectively than conventional steel cable restrainers. The large elastic strain range of the SMA restrainers makes them undergo large deformations while remaining elastic. Furthermore, the pseudoelastic properties of the SMA restrainers result in energy dissipation at the hinges. SMA wires are used to actuate control surfaces of the flying vehicles [4]. Saadat et al. reported several experimental and analytical studies of the SMA devices for structural vibration control [5]. Development of innovative techniques for the restoration of cultural heritage structures by using Nitinol wires has been reported in Italy [5]. Nitinol medical guide wires and some of the SMA medical devices are long and thin elements that pass into the body through a natural opening or a small incision. SMA beams in the above applications may be subjected to moving loads when they are in the operating conditions.

On the other hand, the dynamic response of a beam subjected to moving loads has been studied extensively in the recent years. Some examples include bridges, piping systems subjected to two-phase flows, beams subjected to pressure waves, and machining operations with high axial speeds. Different studies have been conducted for the analysis of the dynamic response of the beams to moving loads [6–9]. The main purposes of this study are as follows:

(1) Presenting a one-dimensional constitutive model for the prediction of SMA mechanical properties in the case of pseudoelasticity.
(2) Providing a dynamical model for the vibration analysis of an SMA beam subjected to a moving load.
(3) Studying the effects of stress-induced phase transformations resulted by the moving load on the loss of stiffness and damping effect of an SMA beam.
(4) Studying the effects of load amplitude and load velocity, type of motion and number of beam constraints on the dynamic response of the beam.
(5) Comparing the dynamic response of an SMA beam and that of an isotropic viscously damped beam.

In the present study, the dynamic response of a continuous simply supported multi-span SMA beam to a constant traveling force with accelerated or decelerated motion or constant velocity motion is analyzed. Investigation of the effects of moving load and SIPT on the dynamic response of the beam is among the main

objectives of the present paper. First, an extended one-dimensional constitutive model is developed to introduce the mechanical behavior of SMA, considering strain as the main variable. Then, Lagrange's equations are applied to analyze the dynamic response of the SMA beam. Also, hysteresis-induced damping capacity and the nonlinear behavior caused by SIPT in an SMA beam subjected to a moving load are analyzed. The constraint conditions of the supports are taken into account using Lagrange's multipliers. To solve Lagrange's equations, trial functions denoting the deflection of the beam is expressed in the polynomial form. Then, the equations are converted into a system of algebraic equations, which is solved by the direct time integration method of Newmark [10]. The results of numerical simulations are presented for single-span and two-span SMA beams with various combinations of speeds, motions, and damping effects.

2. One-dimensional model for pseudoelastic SMAs

Due to the applications of SMAs, many constitutive models have been proposed for simulation of the pseudoelastic and the shape memory effects of SMAs. In this paper, Auricchio's model [11] is applied to reproduce the SMA pseudoelastic behavior. This model is based on a single-scalar internal variable—the volumetric martensite fraction. First, the evolutionary equations of the conversion process of the austenite phase into martensite ($A \rightarrow S$) and the martensite phase into austenite ($S \rightarrow A$) are developed as follows [11]:

$$\sigma_s^{AS} \langle |\sigma| \langle \sigma_f^{AS}, |\dot{\bar{\sigma}}| \rangle 0 : \quad \dot{\xi}_S = -(1-\xi_S)\frac{|\dot{\bar{\sigma}}|}{|\sigma| - \sigma_f^{AS}}, \tag{1}$$

$$\sigma_f^{SA} \langle |\sigma| \langle \sigma_s^{SA}, |\dot{\bar{\sigma}}| \langle 0 : \quad \dot{\xi}_S = \xi_S \frac{|\dot{\bar{\sigma}}|}{|\sigma| - \sigma_f^{SA}}. \tag{2}$$

The overall equivalent modulus for the uniaxial state of stress using the Reuss scheme is given by

$$E = \frac{E_A}{1 + ((E_A/E_S) - 1)\xi_S}.$$

Eqs. (1) and (2) are solved by using the backward-Euler scheme and a return-map algorithm, and ξ_S is calculated.

3. Partial loading and unloading

Fig. 1 shows the outer and inner hysteresis loops for a NiTi alloy. If the stress–strain state during loading or unloading is in the outer hysteresis loop (Fig. 1), Muller's method can be used to describe the behavior of the

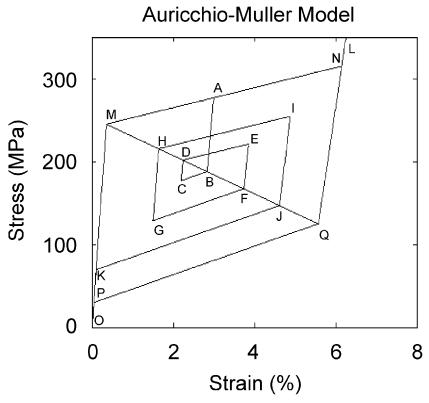

Fig. 1. NiTi alloy, inner and outer hysteresis loops.

SMA [12]. The hysteresis loop contains meta-stable states that lose their (meta-) stability on a line defining unstable phase equilibrium called the trigger line (line MQ in Fig. 1). Thomson et al. [13] explained Muller's idea as follows:

Trigger line is the diagonal of the outer hysteresis loop. If loading is started from the lower left corner of the inner loop (e.g., point G in Fig. 1), there are elastic responses until the trigger line is reached (e.g., line GH in Fig. 1). Then it is followed by inelastic responses as the austenite to martensite transformation proceeds (e.g., line HI in Fig. 1). Similarly, for unloading from the upper right corner (e.g., point I in Fig. 1), there are elastic responses until the trigger line is reached (e.g., line IJ in Fig. 1). Then it is followed by inelastic responses as the martensite transforms to austenite (e.g., line JK in Fig. 1). In the elastic region, there is no phase transformation and Young's modulus of SMA remains constant. Inelastic behavior is due to transformation from austenite to martensite in loading, or from martensite to austenite in unloading.

4. Auricchio–Muller extended model

For a typical NiTi alloy, the material properties obtained from the experimental measurements [14] are as follows:

$$\rho = 6450\,\mathrm{kg\,m^{-3}}, \quad E_A = 69.6\,\mathrm{GPa}, \quad E_S = 33.1\,\mathrm{GPa}, \quad \varepsilon_L = 5{-}8\%,$$
$$\sigma_s^{AS} = 245\,\mathrm{MPa}, \quad \sigma_f^{AS} = 315\,\mathrm{MPa}, \quad \sigma_s^{SA} = 125\,\mathrm{MPa}, \quad \sigma_f^{SA} = 30\,\mathrm{MPa},$$

where ε_L is maximum residual strain.

Auricchio's model is applied to compute stress, Young's modulus, and martensite fraction for loading or unloading case. Muller's model is used to determine the start and end of yielding and recovery and also the elastic response inside the hysteresis loop. Fig. 1 is resulted by implementation of the Auricchio–Muller (AM) extended model. It shows partial loadings and unloadings until total strain recovery is achieved. Solution algorithm of the AM model is as follows:

(1) Input data
(2) Detect loading or unloading for the present strain step at t_{n+1}
  (2.1) In case of loading
    (2.1.1) If there is no phase transformation
      – Strain varies along the line OM ($\xi_S = 0$, $E = E_A$) or
      – Strain varies on the lower triangle, e.g., the line CD (E and ξ_S are constant)
    (2.1.2) If there is full phase transformation
      – Strain varies along the line QL ($\xi_S = 1$, $E = E_S$)
    (2.1.3) If there is partial phase transformation ($A \rightarrow S$)
      – Strain varies along the line MN or
      – Strain varies on the upper triangle, e.g., the line DE
  (2.2) In case of unloading
    (2.2.1) If there is no phase transformation
      – Strain varies along the line OM ($\xi_S = 0$, $E = E_A$) or
      – Strain varies on the upper triangle, e.g., the line AB (E and ξ_S are constant)
    (2.2.2) If there is full phase transformation
      – Strain varies along the line LQ ($\xi_S = 1$, $E = E_S$) or
    (2.2.3) If there is partial phase transformation ($S \rightarrow A$)
      – Strain varies along the line QP or
      – Strain varies on the lower triangle, e.g., the line BC
(3) Compute dissipation energy, potential energy, loss factor, and equivalent damping ratio.

It is observed that the prediction of SMA pseudoelastic behavior by the introduced model is in a good agreement with the two main adopted models [11,12].

5. Dynamical model of the beam

A continuous SMA beam with N supports subjected to a concentrated constant amplitude-moving load is shown in Fig. 2. In order to perform the dynamical analysis of the SMA beam, the following items are required:

- A pseudoelastic model (previously described).
- Young's modulus and equivalent damping ratio of the SMA beam.
- The bending vibration equation of the SMA beam.

5.1. Pseudoelastic model

The following assumptions are considered for the AM model:

- The behavior of phase transition in tension-compression is symmetrical and the stress–strain curve in compression can be considered similar to that in tension [15]. Tension-compression asymmetry has no significant influence on the shape of the global load-deformation hysteresis loop. However, the asymmetry causes the movement of the neutral plane in the case of bending [16].
- If an SMA rod is subjected to a cyclic loading, stress–strain curve, initial and final stress thresholds of the phase transformations are stabilized after a certain number of loading [17]. In this paper it is assumed that SMA is a fully trained material and its properties are stabilized.
- The vibration of SMA is carried out in isothermal conditions.

5.2. Young's modulus and equivalent damping ratio

Stress-induced phase transformation ($A \rightarrow S$) causes stiffness reduction. Thus, pseudoelastic model introduces a new value of Young's modulus of SMA after each time (strain) step. This value must be applied in the next step of calculations. Collet used an equivalent complex Young's modulus in the vibration equations of SMA [2]. In this paper, Young's modulus and loss factor of SMA are calculated separately in two different ways. Auricchio's model is applied for determining Young's modulus, stress, and martensite fraction. The method of Piedboeuf and Gauvin [15] is a suitable method for calculating loss factor and dimensionless equivalent damping ratio in this study.

The main parameters for calculating loss factor are dissipated energy in a cycle and the maximum potential energy [15]. These parameters are shown in Fig. 3. Accordingly, loss factor is defined as

$$\eta = \left(\frac{1}{2\pi}\right)\frac{2\Delta W}{U}, \tag{3}$$

where ΔW (J m^{-3} cycle^{-1}) is the dissipated energy in a cycle and equals the area of the hysteresis loop. U is the maximum potential energy. In the case of no cyclic deformation, dissipated energy should be considered corresponding to ε_{max}. Loss factor is usually defined for a full cyclic deformation in tension-compression. In cyclic loading, the total dissipated energy is equal to twice the dissipated energy in tension. For linear viscoelastic materials with low damping, U is equal to $(1/2)\varepsilon_{max}\sigma_{max}$, but for a nonlinear material, a more precise definition is

$$U = W - \tfrac{1}{2}\Delta W,$$

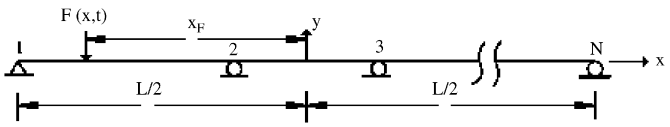

Fig. 2. A continuous SMA beam with N supports.

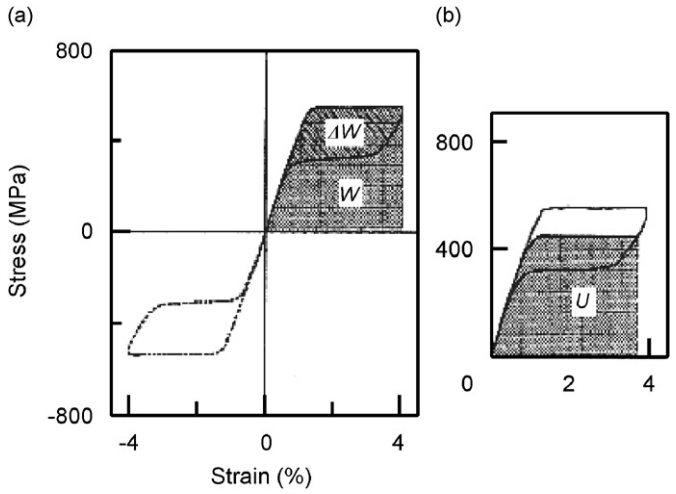

Fig. 3. Pseudoelastic stress–strain curve (a) W, ΔW, (b) U.

where W is the maximum strain energy at $\varepsilon_{\max}$ (Fig. 3). These values are determined through numerical integration. If the excitation frequency equals the natural frequency of the system, the following relation is applied:

$$\eta = 2\xi. \tag{4}$$

This relation is usually used for the estimation of a viscoelastic material damping [18]. In this paper Eq. (4) is used for calculating the equivalent damping ratio of the SMA beam. Equivalent damping ratio of the kth vibration mode ξ_k is as follows:

$$\xi_k = \frac{\gamma_e + \gamma_i \omega_k^2}{2\omega_k}, \tag{5}$$

where γ_e and γ_i are the proportional constants of the external and internal damping and ω_k is the natural circular frequency of the kth mode [7]. The external and internal dampings (r_e and r_i) are assumed to be proportional to the mass and stiffness properties of the beam, respectively:

$$r_e = \gamma_e \mu, \quad r_i = \gamma_i EI(x) \tag{6}$$

where μ and EI denote the mass per unit length and the flexural rigidity of the beam, respectively. It is known that the external damping is very small compared with the internal damping. Therefore, ignoring γ_e and substituting Eq. (6) into Eq. (5), for the first natural circular frequency results in

$$r_i = \frac{2EI(x)\xi_1}{\omega_1}. \tag{7}$$

For a given vibration cycle, η should be calculated, first. Then, ξ and r_i are obtained by using Eqs. (4) and (7).

According to the magnitude of moving load and its positive or negative distance from a given point on the beam, the austenite phase evolutionary process to martensite ($A \rightarrow S$) or the martensite phase evolutionary process to austenite ($S \rightarrow A$) occurs. So σ, ε, E, and ξ will change.

Fig. 4 shows the change of equivalent damping ratio in terms of maximum strain. It should be noted that the increase of strain after full phase transformation ($A \rightarrow S$) (point N in Fig. 1) decreases the equivalent damping ratio. Fig. 5 shows the variations of E versus ξ_S. In this figure, according to the Reuss model [11], nonlinear dependence of E on the martensite fraction is indicated. Variations of the first natural frequency, Young's modulus, and equivalent damping ratio for the midpoint of a simply supported beam acted upon by a concentrated moving force movements are presented in Table 1.

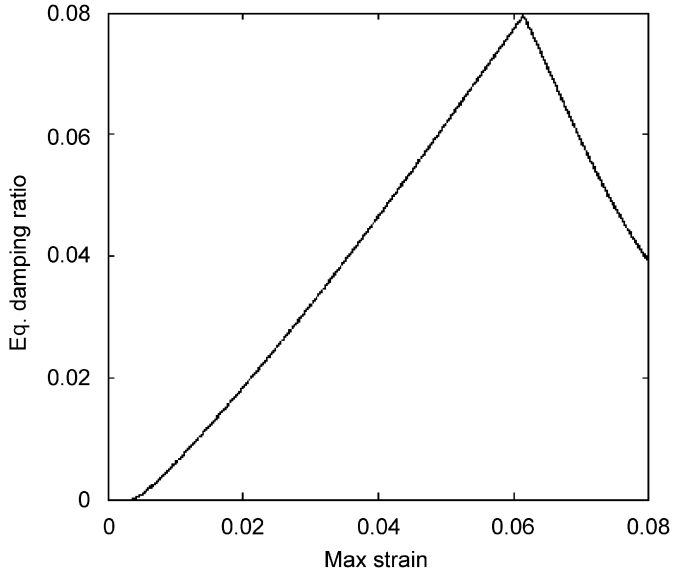

Fig. 4. Equivalent damping ratio versus maximum strain.

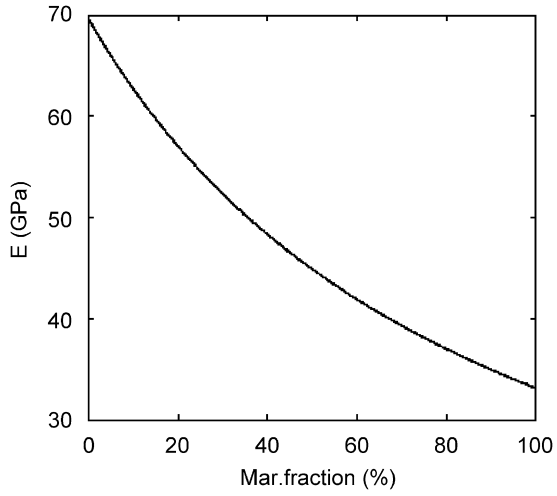

Fig. 5. Young's modulus of SMA versus martensite fraction.

Table 1
First natural frequency, Young's modulus and equivalent damping ratio of the midpoint of a simply supported SMA beam due to decelerated motion of the moving load, $\alpha = 1.0$ and $F_0 = 1500\,\mathrm{N}$

Load dimensionless position	−0.50	−0.32	−0.16	−0.02	0.11	0.21	0.31	0.38	0.43	0.47	0.49	0.50
First natural frequency (rad s^{-1})	146.2	146.2	146.2	146.2	130.8	123.7	119.2	112.7	111.7	111.7	111.7	128.1
Young's modulus (GPa)	69.6	69.6	69.6	55.7	49.8	46.2	41.3	40.6	40.6	40.6	53.4	69.6
Equivalent damping ratio	0	0	0	0.014	0.024	0.032	0.046	0.048	0.048	0.048	0.048	0.048

5.3. Lagrange's equations

In the present study, Lagrange's equations are used for analyzing the dynamic response of the SMA beam subjected to a moving load. The concentrated load moves from the left-hand side of the beam at the point

$x = -(L/2)$ towards the right-hand side of the beam at the point $x = L/2$ (Fig. 2). The constraint conditions of the supports are taken into account by using Lagrange's multipliers. All transverse deflections take place in the xy plane.

The kinetic energy of the beam in Cartesian coordinates at any time is

$$T = \frac{1}{2}\int_{-L/2}^{L/2} \rho A \left(\frac{\partial w(x,t)}{\partial t}\right)^2 \mathrm{d}x,$$

where ρ and A are mass density and cross-section area, respectively. Moreover, elastic strain energy of the beam at any time is

$$U = \frac{1}{2}\int_{-L/2}^{L/2} EI \left(\frac{\partial^2 w(x,t)}{\partial x^2}\right)^2 \mathrm{d}x.$$

Also the dissipation energy of the beam at any time is as follows:

$$R = \frac{1}{2}\int_{-L/2}^{L/2} r_i \left(\frac{\partial^2 \dot{w}(x,t)}{\partial x^2}\right)^2 \mathrm{d}x.$$

The potential energy of the external force $F(x,t)$ is $V = -F(x,t)\cdot w(x_F,t)$, where $F(x,t)$ is defined by Eq. (14). For applying Lagrange's equations, the trial function $w(x,t)$ is approximated by space-dependent polynomial terms of $x^0, x^1, x^2, \ldots, x^m$ and time-dependent generalized coordinates of $p_m(t)$ [9].Thus

$$w(x,t) = \sum_{m=0}^{M} p_m(t) x^m. \tag{8}$$

The constraint conditions for simply supported ends and intermediate constraints of the beam are applied as follows:

$$\lambda_i w(x_{si},t) = 0, \quad i = 1,2,3,\ldots,N, \tag{9}$$

where x_{si} denotes the location of the ith support and N denotes the number of supports. In Eq. (9) λ_i values are Lagrange's multipliers, indicating the supports reactions.

Lagrangian function with Lagrange's multipliers is

$$L = T - (U + V) + \lambda_i w(x_{si},t), \quad i = 1,2,3,\ldots,N. \tag{10}$$

The generalized damping force Q_D can be obtained by differentiating R with respect to $\dot{p}_k$ as follows:

$$Q_D = -\frac{\partial R}{\partial \dot{p}_k}, \quad k = 1,2,3,\ldots M+N,$$

where $\dot{p}_k$ is the derivative of p_k with respect to time. Then, by using Lagrange's equations as

$$\frac{\partial L}{\partial p_k} - \frac{\mathrm{d}}{\mathrm{d}t}\frac{\partial L}{\partial \dot{p}_k} + Q_D = 0, \quad k = 1,2,3,\ldots,M+N$$

and introducing

$$p_{M+i} = \lambda_i, \quad i = 1,2,3,\ldots,N,$$

our problem yields the following equation:

$$[\mathbf{A}]\{\mathbf{p}_m\} + [\mathbf{B}]\{\dot{\mathbf{p}}_m\} + [\mathbf{C}]\{\ddot{\mathbf{p}}_m\} = \{\mathbf{D}\}, \quad m = 1,2,3,\ldots,M+N, \tag{11}$$

where

$$A_{km} = \int_{-L/2}^{L/2} EI(x)(x^k)''(x^m)'' \,\mathrm{d}x, \quad k,m = 1,2,3\ldots,M,$$
$$A_{km} = x_{sm}^k, \quad k = 1,\ldots,M;\ \ m = M+1,\ldots M+N,$$
$$A_{km} = x_{sk}^m, \quad k = M+1,\ldots,M+N;\ \ m = 1,\ldots,M,$$
$$A_{km} = 0, \quad k,m = M+1,\ldots,M+N$$

$$B_{km} = \int_{-L/2}^{L/2} r_i(x^k)''(x^m)'' \,\mathrm{d}x, \quad k,m = 1,2,3,\ldots,M,$$

$$B_{km} = 0, \quad \begin{cases} k = 1,\ldots,M, & m = M+1,\ldots,M+N, \\ k = M+1,\ldots,M+N, & m = 1,\ldots,M, \end{cases}$$

$$C_{km} = \int_{-(L/2)}^{L/2} \rho A(x) x^k x^m \,\mathrm{d}x, \quad k,m = 1,2,3,\ldots,M,$$
$$C_{km} = 0, \quad \begin{cases} k = 1,\ldots,M, & m = M+1,\ldots,M+N, \\ k = M+1,\ldots,M+N, & m = 1,\ldots,M, \end{cases}$$
$$D_k = Fx_0^k, \quad k = 1,2,3,\ldots,M,$$
$$D_k = 0, \quad k = M+1,\ldots,M+N,$$

and $(x^k)''$ is second derivative of x^k with respect to x. The matrices [**A**], [**B**], [**C**] are independent of time, but vector {**D**} depends on time. Eq. (11) is solved by the direct time integration method of Newmark [10], and $p_m, \dot{p}_m, \ddot{p}_m$, and λ_i coefficients are obtained for any time t. Then, the displacement, velocity, and acceleration at the considered point and time can be determined by using Eq. (8).

Strain is assumed to be linear along the beam thickness and according to the Euler–Bernoulli approach, it can be written as

$$\varepsilon_x = -y\frac{\partial^2 w(x,t)}{\partial x^2}.$$

Time-dependent generalized coordinates can be expressed as follows:

$$p_m(t) = \bar{p}_m \mathrm{e}^{\mathrm{i}\omega t}. \tag{12}$$

By substituting Eq. (12) into Eq. (11) and taking the damping matrix of the beam [**B**] and the external forces {**D**} as zero, a set of linear homogeneous equations in the following matrix form is obtained:

$$[\mathbf{A}]\{\bar{\mathbf{p}}_m\} - \omega^2[\mathbf{C}]\{\bar{\mathbf{p}}_m\} = \{\mathbf{0}\}, \tag{13}$$

where ω is the natural frequency of the beam. By calculating eigenvalues, ω_i, of Eq. (13), the natural frequencies of the beam are determined. This calculation is repeated in each time step. Typically, first natural frequency, Young's modulus, and equivalent damping ratio for the midpoint of a simply supported SMA beam during force movement are shown in Table 1.

6. Numerical results and discussion

A computer program in MATLAB is developed for studying the dynamical behavior of a pseudoelastic SMA beam subjected to a moving load. Four subprograms are developed for the following purposes:

(a) Calculation of the matrices [**A**], [**B**], [**C**] and {**D**} for solving Eq. (11) in the consecutive time steps during the movement of the concentrated load.
(b) Calculation of deflection and strain at any given point on the SMA beam by Newmark's method.

Table 2
Convergence study of the natural frequencies of the SMA beam

No. of terms	ω_1 (rad s^{-1})	ω_2 (rad s^{-1})	ω_3 (rad s^{-1})	ω_4 (rad s^{-1})
5	146.2792	743.7970	1953.0382	–
6	146.2792	587.4200	1953.0382	4089.7627
8	146.2359	584.9541	1338.5040	2438.4802
10	146.2359	584.9435	1316.4449	2342.9084
12	146.2359	584.9435	1316.1244	2339.8109
19	146.2359	584.9435	1316.1228	2339.7739

(c) Determination of the martensite fraction, Young's modulus and stress at any given point on the beam by the AM extended model.
(d) Calculation of the loss factor and dimensionless equivalent damping ratio.

At this stage, a convergence study for determining the number of polynomial terms in Eq. (8) is carried out. For this purpose, the natural frequencies of the considered beam for the case of full austenite phase are determined by Eq. (13). The calculated natural frequencies are compared with those determined by the related formula of Ref. [19] in Table 2. It is observed that a good convergence for the first natural frequency is achieved with 12 polynomial terms.

6.1. A single-span SMA beam

The analysis is applied to a simply supported SMA beam .The cross-section area (A) and the length of the beam (L) are 100 mm^2 and 0.8 m. The beam is subjected to a concentrated constant amplitude load. Material properties are described previously. Strain is computed for the external layer of the beam cross-section. The load $F(x,t)$ is written as [9]

$$F(x,t) = \delta(x - f(t))F_0, \tag{14}$$

where $\delta(.)$ denotes Dirac delta function and $f(t)$ denotes a time function describing the type of the force motion as $f(t) = x_i + c_i t + (1/2)at^2$, where x_i is the positive or negative initial distance of the force from the midpoint of the beam, c_i is the initial speed, and a is the acceleration of motion. Uniform decelerated or accelerated motions are described with the above function. The time function for the uniform velocity is introduced by $f(t) = x_i + c_i t$.

The required time for reaching the force at the right-hand side of the beam is t_L. c_f is considered as the final speed of the moving force at the end of the beam. x_i, c_i, c_f, a, and t_L for three types of motions are given in Table 3.

Fryba [20] denotes the circular frequency at the nth mode of vibration of an isotropic simply supported beam by

$$\omega_n^2 = \left(\frac{n\pi}{L}\right)^4 \frac{EI}{\mu}, \tag{15}$$

and the circular frequency by

$$\omega = \frac{\pi c}{L}. \tag{16}$$

Effect of moving load velocity is introduced by the dimensionless speed parameter, α [20], which is defined as

$$\alpha = \frac{\omega}{\omega_1}. \tag{17}$$

Table 3
Kinematical parameters for various types of motions

Type of motion	x_i	c_i	c_f	a	t_L
Accelerated motion	$-L/2$	0	c	$c^2/2L$	$2L/c$
Decelerated motion	$-L/2$	c	0	$-c^2/2L$	$2L/c$
Uniform velocity motion	$-L/2$	c	c	0	L/c

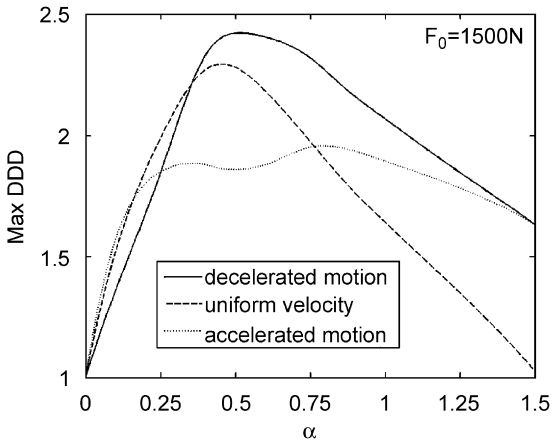

Fig. 6. Maximum DDD at the midpoint of a simply supported SMA beam versus α.

For the first mode of vibration, by substituting Eqs. (15), (16) into Eq. (17), it can be concluded that

$$\alpha = \frac{cL}{\pi}\left(\frac{\mu}{EI}\right)^{1/2}.$$

The new symbol c_{cr} is defined as

$$c_{cr} = \frac{\omega_1 L}{\pi} = \frac{\pi}{L}\left(\frac{EI}{\mu}\right)^{1/2}.$$

So, it can be written that

$$\alpha = \frac{c}{c_{cr}}.$$

For $\alpha = 1$, when the load is leaving a simply supported beam, dimensionless dynamic deflection at the midpoint of the beam has maximum value with respect to other values of α. ω_1 equals 146.23 rad s^{-1} for the given beam. If the force value is high enough, Young's modulus and the first natural frequency of the SMA beam will change due to the conversion process of the austenite phase into the martensite phase.

Figs. 6 and 7 show maximum DDD, $w((L/2),t)/w_{st}$ and maximum dimensionless equivalent damping ratio (ξ) at the midpoint of beam, versus α. For the considered beam, w_{st} equals $F_0L^3/48E_AI$. Ten different values from 0.1 to 1.5 are adopted for α in each type of motion. The moving force value is considered 1500 N. The maximum DDD in the decelerated motion has a higher value than the other types of motions. This result is in perfect agreement with that given in Ref. [7]. Also, it is seen in Fig. 6 that max DDD occurs for $\alpha = 0.5$. Fig. 7 shows that the maximum value for ξ, 0.063 is related to decelerated motion and $\alpha \approx 0.5$. Young's modulus in this case is 36.7 GPa. For the large part of the α-axis, the maximum value of ξ belongs to the decelerated motion. Two different cases are studied to show the damping effect. In the first case, damping property is considered for the SMA beam and in the second case its damping property is neglected. Damping effect (ΔD) is represented by the difference between DDD of the undamped case and that of the damped case.

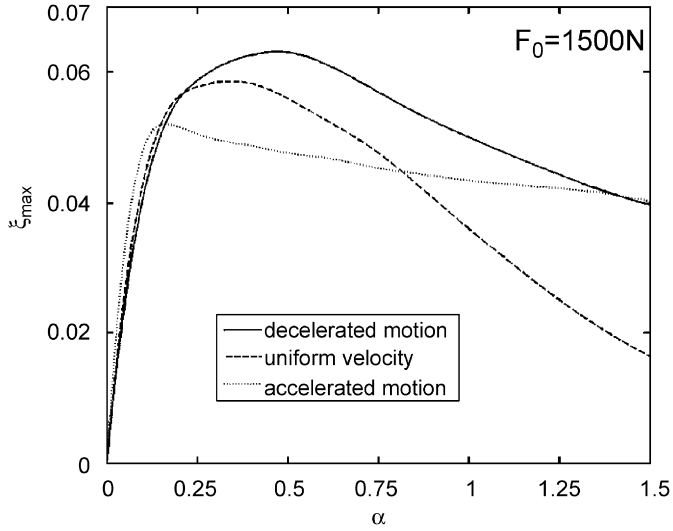

Fig. 7. Maximum ξ at the midpoint of the SMA beam versus α.

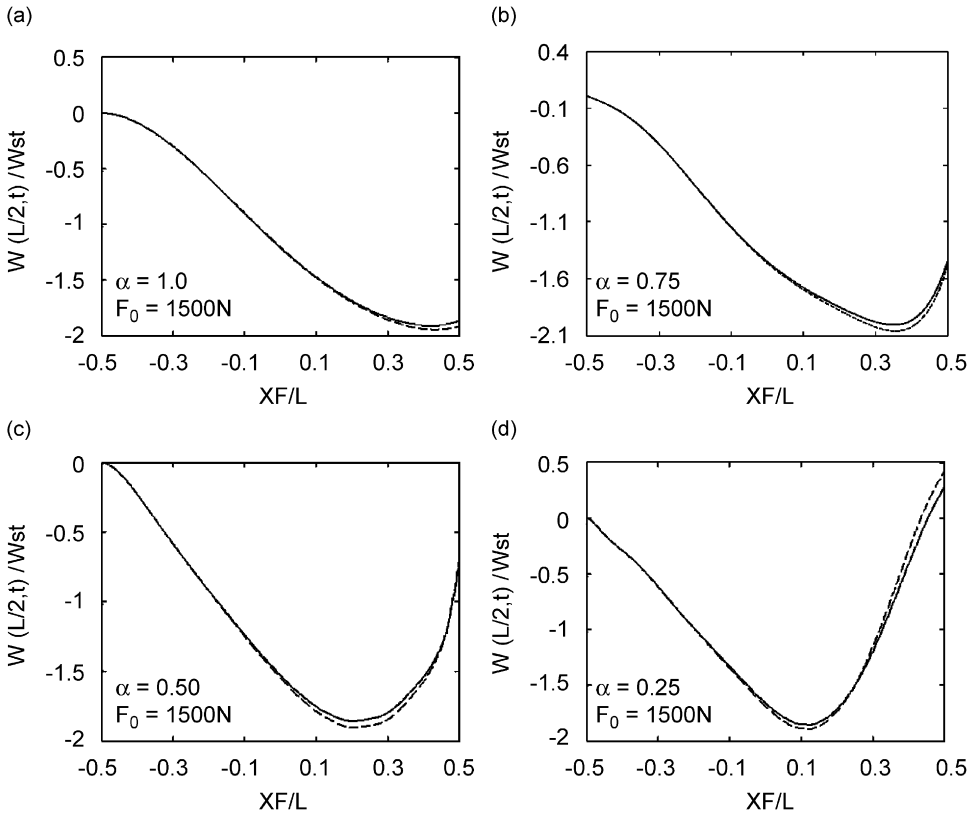

Fig. 8. DDD at the midpoint of the SMA beam versus the dimensionless position of moving load with accelerated motion and four values of α; (- - -) undamped oscillations and (—) damped oscillations.

Figs. 8(a–d), 9(a–d), and 10(a–d) show DDD at the midpoint of the beam, versus the dimensionless parameter of the force position along the beam, x_F/L. They show results for four values of speeds, $\alpha = 1.0$, 0.75, 0.5, and 0.25, respectively, in each type of the motion. The difference between dynamic deflections of the

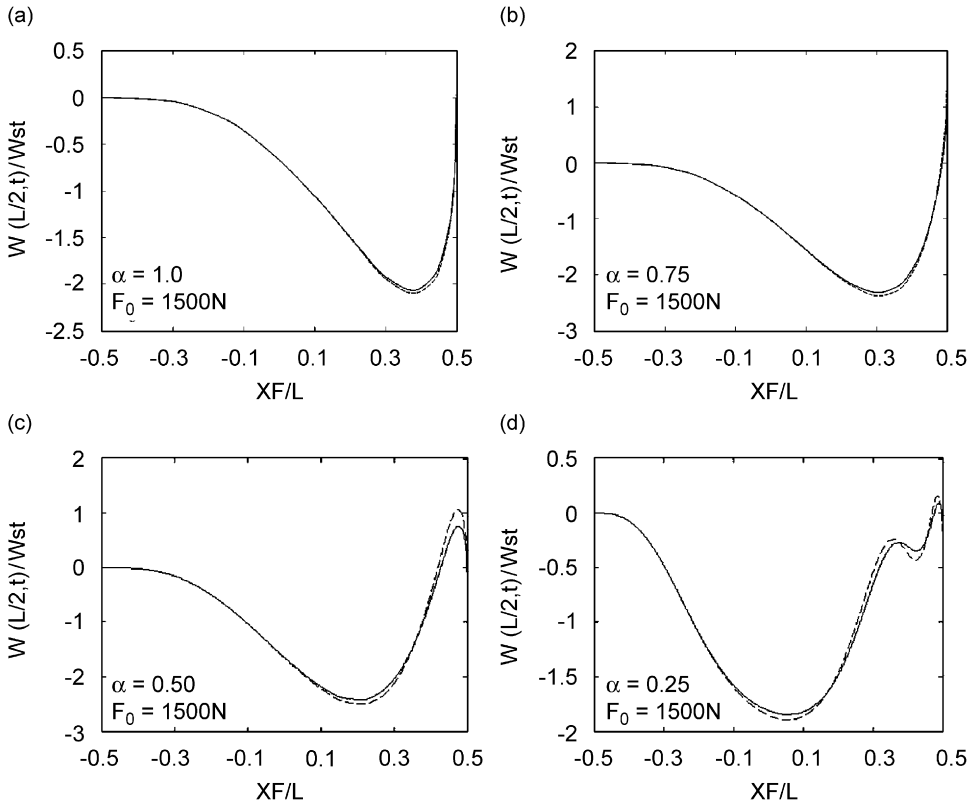

Fig. 9. DDD at the midpoint of the SMA beam versus the dimensionless position of moving load with decelerated motion and four values of α; (- - -) undamped oscillations and (—) damped oscillations.

different types of motions depends on the kinematics of motion and SIPT. It is worth noting that negative displacement means compressive stress at the top of the beam. Number of oscillations in the decelerated motion is more than that in the other cases. In each type of motion, as velocity increases, position of the moving load corresponding to the maximum DDD moves towards the right-hand side of the beam. These results are in good agreement with those given in Ref. [7]. More damping effects in all types of motion are achieved for less values of speed. On the other hand, by comparing DDD for different values of α, increase of DDD in the lower speed case of the decelerated motion is faster than that in the higher speed cases, because in the lower speed, phase transformation process $A \rightarrow S$ occurs more rapidly than higher speeds at the beginning of the force movement.

Figs. 11(a–d) show DDD of a simply supported SMA beam for decelerated motion and $\alpha = 0.25$. The relevant force values are 2000, 1000, 500, and 50 N, respectively. Increase of force value causes more phase transformation and there are higher damping effect and higher reduction of Young's modulus for the higher value of load. The maximum equivalent damping ratio and the minimum Young's modulus corresponding to the mentioned cases are shown in Table 4. It is observed that by increasing the force value, the maximum DDD increases and the load position corresponding to the maximum DDD moves towards the right-hand side of the beam. On the other hand, there is higher damping effect for the higher load value. Also, increase of the force value reduces the number of oscillations. Therefore, reduction of fatigue effect and longer service life are expected. Fig. 11a shows that the position of the moving load corresponding to the maximum DDD for the damped and undamped conditions are slightly different and the relevant values are 0.077 and 0.076. This difference is due to the damping effect on the beam resonance frequency.

It is worth noting that an isotropic beam with viscous damping has a simple response, which does not depend on the moving load value. But the behavior of an SMA beam depends on the magnitude

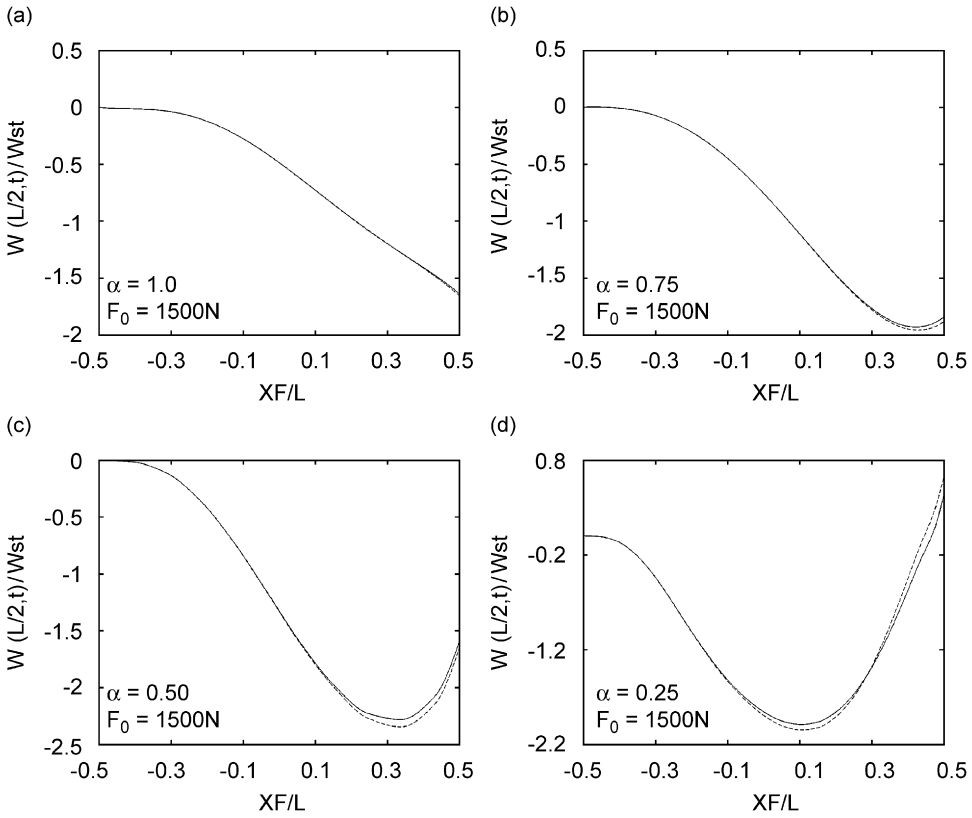

Fig. 10. DDD at the midpoint of the SMA beam versus the dimensionless position of moving load with uniform velocity and four values of α; (- - -) undamped oscillations and (—) damped oscillations.

of the moving load. An SMA beam represents various Young's modulus, damping effects and vibration frequencies during the oscillations. So SMA can be regarded as a smart material. Dynamical behavior of a simply supported isotropic viscously damped beam can be compared with the behavior of the SMA beam. The DDD at the midpoint of the viscously damped beam is shown in Fig. 12. Two equivalent damping ratios 0.0 and 0.079 are applied for representing damping effects on the beam. Defining $\Delta D = D_1 - D_2$, the dimensionless damping effect can be considered as $\Delta D/D_1$. The maximum DDD corresponding to the above equivalent damping ratio, ΔD, and $\Delta D/D_1$ of the isotropic beam are shown in Table 5.

In the SMA beam, the equivalent damping ratio corresponding to the moving load value of 2000 N reaches a maximum value of 0.079. This condition corresponds to point N on the outer hysteresis loop in Fig. 1. The above parameters for the SMA beam subjected to a moving load of 2000 N are also shown in Table 5. These results are for decelerated motion of moving load with $\alpha = 0.25$. Higher values of maximum DDD and lower value of $\Delta D/D_1$ for the SMA beam are due to the phase transformation process $A \rightarrow S$. Hence, for a large part of the force movement on the beam, equivalent damping ratio and Young's modulus of the adopted point are less than 0.079 and E_A. Behavior of the SMA beam subjected to the force value of 50 N (Fig. 11d) is similar to the isotropic viscously damped beam behavior with $\xi = 0$ (Fig. 12). Because of too little force value, there is no phase transformation in the SMA beam.

6.2. A two-span beam

A two-span SMA beam with simply supported ends and an intermediate point constraint is considered (Fig. 13). The geometrical and mechanical properties of the beam are as the single-span SMA beam considered

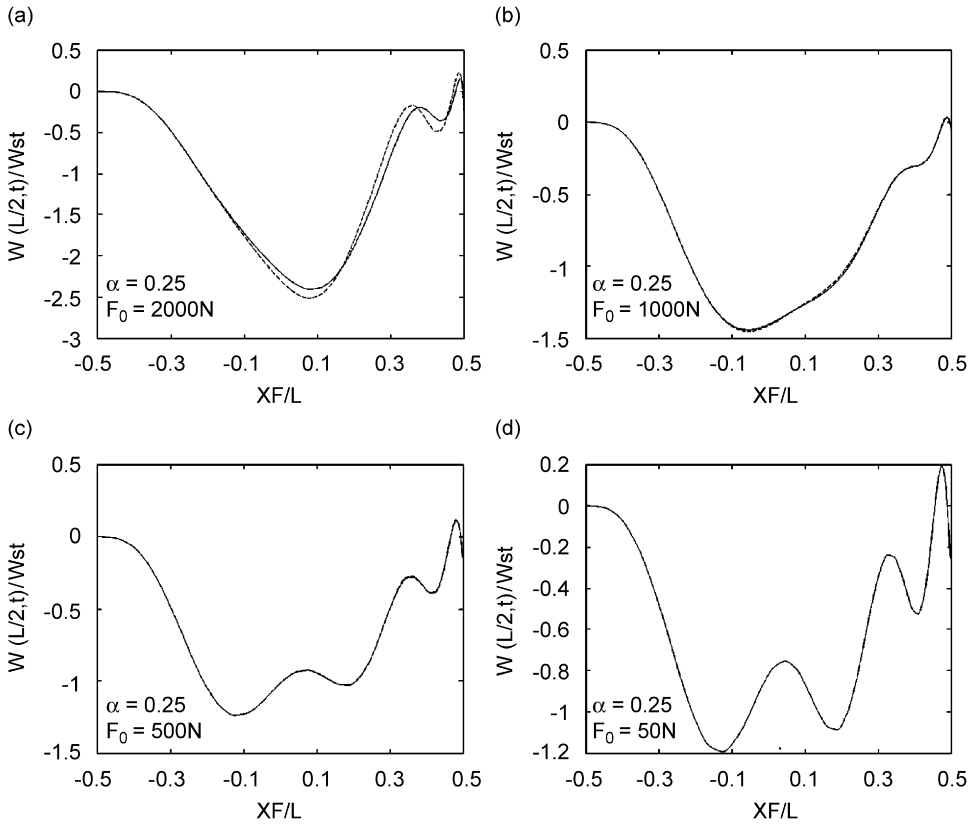

Fig. 11. DDD at the midpoint of the SMA beam versus the dimensionless position of the moving load with accelerated motion, $\alpha = 0.25$, and varying F_0; (- - -) undamped oscillations and (—) damped oscillations.

Table 4
Maximum equivalent damping ratio, minimum Young's modulus and maximum DDD at the midpoint of a simply supported SMA beam due to decelerated motion of the moving load, $\alpha = 0.25$ and various values of load

Load (N)	2000	1000	500	50
Max equivalent damping ratio	0.079	0.022	0.005	0
Min Young's modulus (GPa)	33.1	51.1	63.1	69.6
Max DDD	2.404	1.441	1.237	1.192

previously. The first natural frequency of the beam in the full austenite phase is $584.85\,\mathrm{rad\,s^{-1}}$ obtained by Eq. (13). Also for this example, the dynamic deflection is normalized by the midpoint static deflection of the simply supported beam: ($w_{st} = F_0L^3/48E_AI$). Fig. 14(a–d) shows the DDD of the point under a moving load (1500 N) with decelerated motion and $\alpha = 1.0,0.75,0.5$, and 0.25, respectively. The decrease of initial speed to $\alpha = 0.5$ causes more phase transformation in the beam. Therefore, the maximum dimensionless equivalent damping ratio of 0.033 and the maximum damping effect of 0.0064 occur in the case of $\alpha = 0.5$. For $\alpha = 1.0$, the damping effect of 0.00057 is very small, because the phase transformation is too little and the SMA beam remains in the austenite phase. In the low velocities of the moving load, by increasing the load velocity, the SMA beam has higher value for the maximum DDD until a certain value of speed. Then, there is a decrease in the DDD with increase in α. DDD of the point under the moving load for the decelerated motion and $\alpha = 0.25$ are shown in Figs. 15(a, b). The applied moving loads are 2000 and 250 N, respectively. Increasing of the force value causes more phase transformation, higher damping effect, less Young's modulus, and higher value for

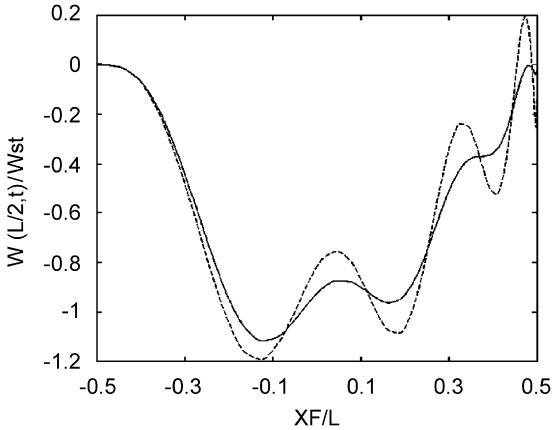

Fig. 12. DDD of a simply supported isotropic viscously damped beam versus the dimensionless position of the moving load with decelerated motion and $\alpha = 0.25$; (- - -) $\xi = 0.0$ and (—) $\xi = 0.079$.

Table 5
Comparison of the maximum DDD and ΔD at the midpoint of the beam subjected to a moving load between a simply supported isotropic viscously damped beam and a simply supported SMA beam

	Max DDD		ΔD	$\Delta D/D_1$
	D_1 for $\xi = 0.0$	D_2 for $\xi = 0.079$		
Viscously damped beam	1.192	1.117	0.075	0.063
SMA beam	2.511	2.404	0.107	0.043

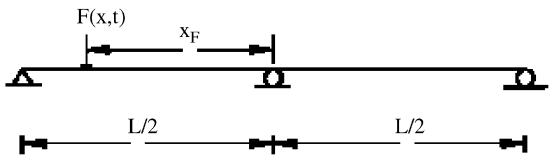

Fig. 13. A two-span SMA beam.

the maximum DDD. Table 6 shows the maximum equivalent damping ratio, minimum Young's modulus, and maximum DDD at the point of the moving load for $F_0 = 250$ and 2000 N. Comparison of similar parameters in Tables 4 and 6 clearly shows that in the case of $F_0 = 2000$ N, maximum equivalent damping ratio and maximum DDD of the two-span SMA beam—0.019 and 0.153—are much smaller than the relevant values of the simply supported SMA beam—0.079 and 2.404. On the other hand, the minimum Young's modulus of the two-span beam, 52.9 GPa, is much more than the relevant value of the single-span beam, 33.1 GPa. Therefore, the number of supports has a strong influence on the dynamic response of the SMA beam subjected to a moving load as expected. This result is consistent with those seen by Lee [6] and Kocaturk [9].

7. Conclusions

The dynamic responses of the simply supported SMA beams subjected to a concentrated moving load were analyzed. Use of an AM extended model and Lagrange's equations with the applied trial function provide a good solution to this problem. Numerical calculations were directed to clarify the effect of concentrated load

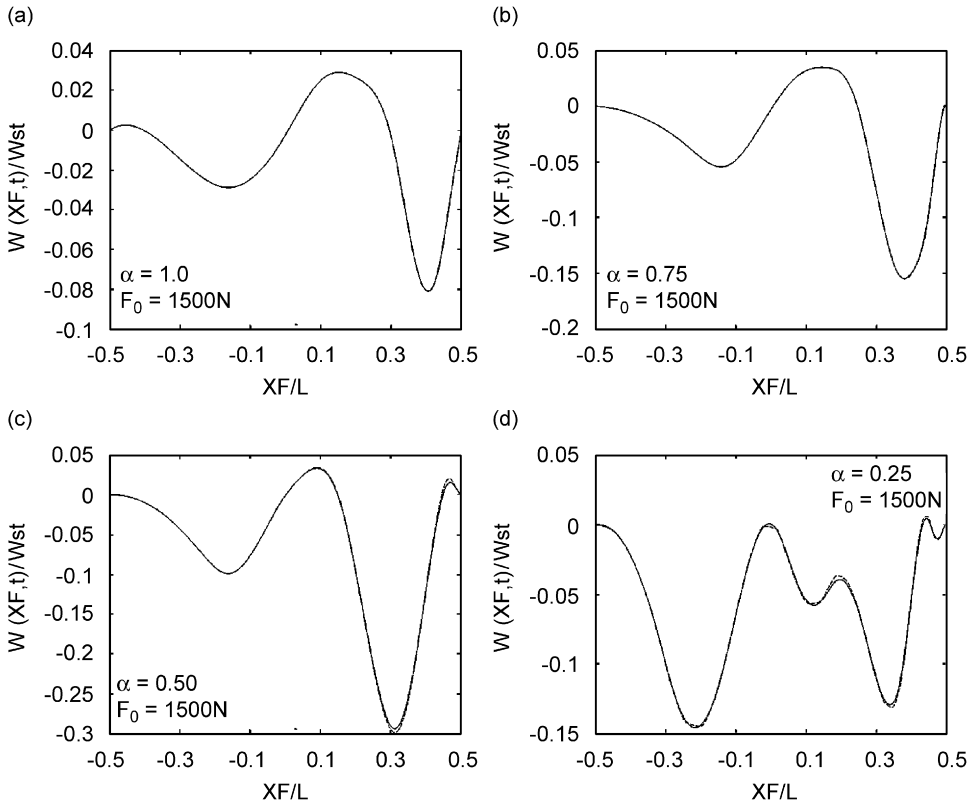

Fig. 14. DDD at the moving load position on a two-span SMA beam versus the dimensionless position of the moving load with decelerated motion, force amplitude of 1500 N and four values for α; (- - -) undamped oscillations and (—) damped oscillations.

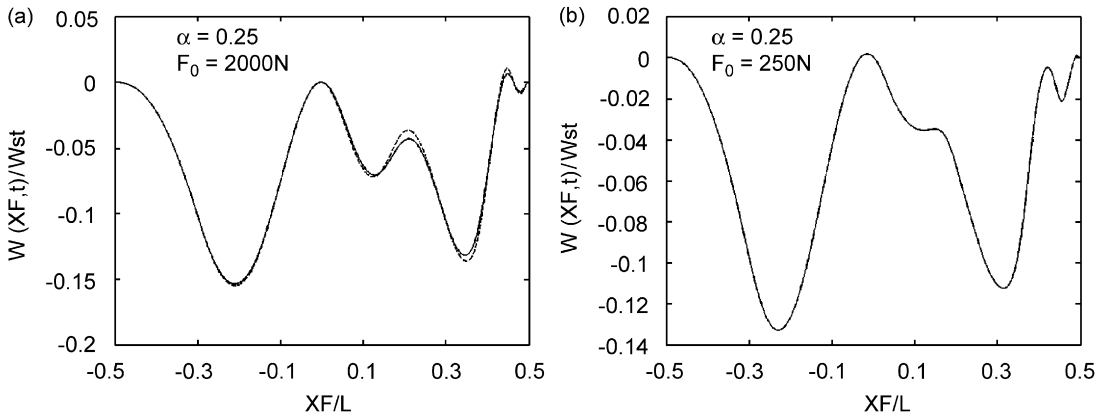

Fig. 15. Dimensionless dynamic deflection of the two-span SMA beam versus the dimensionless position of the moving load with decelerated motion, $\alpha = 0.25$ and two values for force amplitude; (- - -) undamped oscillations and (—) damped oscillations.

velocity, type of motion, force amplitude, and constraints of the beam. The most important results are as follows:

(1) Unlike the isotropic viscously damped beam, behavior of the SMA beam changes with respect to the moving load value. It means that SMA acts as a smart material. It clearly appears that the dynamical behavior of the SMA beam is significantly nonlinear.

Table 6
Maximum equivalent damping ratio, minimum Young's modulus and maximum DDD at the position of a moving load with decelerated motion on a two-span SMA beam, two values for F_0 and $\alpha = 0.25$

Load (N)	250	2000
Max equivalent damping ratio	0	0.019
Min Young's modulus (GPa)	69.6	52.9
Max DDD	0.132	0.153

(2) Higher values of the moving load cause more damping effect and less Young's modulus of the SMA.
(3) In each type of motion, damping effect depends on the load speed.
(4) The maximum DDD and the maximum damping effect are achieved for the decelerated motion and a certain value for the load velocity.
(5) The number of oscillations for the decelerated motion and smaller values of the moving load are more than those of the other cases.
(6) DDD and damping effect of the two-span SMA beam are very small compared with those of the single-span beam.

References

[1] S. Saadat, M. Noori, H. Davoodi, Z. Hou, Y. Suzuki, A. Masuda, Using NiTi SMA tendons for vibration control of coastal structures, *Smart Materials and Structures* 10 (2001) 695–704.
[2] M. Collett, E. Foltete, C. Lexcellent, Analysis of the behavior of a shape memory alloy beam under dynamical loading, *European Journal of Mechanics A/Solids* 20 (2001) 615–630.
[3] R. Des Roches, M. Delemant, Seismic Retrofit of simply supported bridges using shape memory alloys, *Engineering Structures* 24 (3) (2002) 325–332.
[4] J.V. Humbeeck, Non-medical applications of shape memory alloys, *Materials Science and Engineering/A* 273–275 (1999) 134–148.
[5] M.O. Moroni, R. Saldivia, M. Sarrazin, A. Sepulveda, Damping characteristics of a CuZnAlNi shape memory alloy, *Materials Science and Engineering/A* 335 (2002) 313–319.
[6] H.P. Lee, Dynamic response of a beam with intermediate point constraints subject to a moving load, *Journal of Sound and Vibration* 171 (1994) 361–368.
[7] M. Abu-Hilal, H.S. Zibdeh, Vibration analysis of beams with general boundary conditions traversed by a moving force, *Journal of Sound and Vibration* 229 (2) (2000) 377–388.
[8] M. Abu-Hilal, M. Mohsen, Vibration of beams with general boundary conditions due to a moving harmonic load, *Journal of Sound and Vibration* 232 (4) (2000) 703–717.
[9] T. Kocaturk, M. Simsek, Vibration of viscoelastic beams subjected to moving harmonic loads, *Journal of Engineering and Natural Sciences* 3 (2004) 116–128.
[10] N.M. Newmark, A method of computation for structural dynamics, *ASCE Journal of Engineering Mechanics Division* 85 (1959) 67–94.
[11] F. Auricchio, E. Sacco, A one-dimensional model for pseudoelastic shape memory alloys with different elastic properties between martensite and austenite, *International Journal of Non-Linear Mechanics* 32 (1997) 1101–1114.
[12] I. Muller, H. Xu, On the pseudo-elastic hysteresis, *Acta Metallurgical Materials* 39 (1991) 263–271.
[13] P. Thomson, G.J. Balas, P.H. Leo, Analysis of trigger line models for shape memory hysteresis based on dynamic testing, *Journal of Intelligent Material System and Structures* 8 (1997) 193–201.
[14] A.J. Zak, M.P. Cartmell, W.M. Ostachowicz, M. Wiercigroch, One-dimensional shape memory alloy models for use with reinforced composite structures, *Smart Materials and Structures* 12 (2003) 338–346.
[15] M.C. Piedboeuf, R. Gauvin, Damping behavior of shape memory alloys: Strain amplitude, frequency and temperature effects, *Journal of Sound and Vibration* 214 (1998) 885–901.
[16] J. Rejzner, C. Lexcellent, B. Raniecki, Pseudolastic behavior of shape memory alloy beams under pure bending: experiments and modeling, *International Journal of Mechanical Sciences* 44 (2002) 665–685.
[17] F. Auricchio, S. Marfia, E. Sacco, Modeling of SMA materials: Training and two way memory effects, *Computers and Structures* 81 (2003) 2301–2317.
[18] D.J. Inman, *Engineering Vibration*, Prentice-Hall Inc., Englewood Cliffs, NJ, 1996.
[19] S.S. Rao, *Mechanical Vibrations*, third ed., Addison-Wesley publishing company, Reading, MA, 1995.
[20] L. Fryba, *Vibration of Solids and Structures Under Moving Loads*, Noordhoff International Publishing, Groningen, The Netherlands, 1972.